PROGRESS IN HIGH EFFICIENCY PROCESSING OF EFG SILICON SOLAR CELLS

M. Kaes[1], G. Hahn[1,2], A. Metz[3], G. Agostinelli[4], Y. Ma[4], J. Junge[1], A. Zuschlag[1], D. Groetschel[1]
[1]University of Konstanz, Department of Physics, P.O.Box X916, 78457 Konstanz, Germany
[2]also with Fraunhofer Institute for Solar Energy Systems (ISE), Heidenhofstr. 2, 79110 Freiburg, Germany
[3]SCHOTT Solar GmbH, Carl-Zeiss-Str. 4, 63755 Alzenau, Germany
[4]IMEC, Kapeldreef 75, B-3001 Leuven, Belgium

Author for correspondence: Martin.Kaes@uni-konstanz.de, Tel.: +497531882082, Fax: +497531883895

ABSTRACT: In contrast to standard block cast multicrystalline material the performance of EFG material is strongly related to an efficient hydrogenation step. In conformance to former publications the temperature profile during firing of a hydrogen-rich PECVD SiN_x layer strongly affects the effectiveness of hydrogenation. With improved firing conditions 17.9% in efficiency could be reached on 2x2 cm² EFG solar cells using a photolithography based solar cell process. Minor improvements are further reached by a better passivated emitter at the front side of the solar cells, raising the efficiency to 18.2 %. In contrast to commonly used texturing methods plasma texturing at IMEC (meanwhile also at Konstanz) is able to further increase efficiencies on EFG material. A new solar cell process is available to replace the full area Al BSF (with moderate surface passivation quality) with a SiO_2/SiN_x stack of good surface passivation quality using laser fired contacts. The process is applicable for multicrystalline material including a good hydrogenation together with a high temperature stable passivation for the rear side. First results are encouraging on untextured solar cells (diced out to 2x2 cm²) resulting in 19.4 % efficiency on floatzone and 18.5 % efficiency on standard block cast multicrystalline material. It is planned to apply this process on EFG material to further increase the maximum efficiency for this material in the future.
Keywords: High-Efficiency, Passivation, Ribbon Silicon

1 INTRODUCTION

The currently used lab-type processing for fabrication of highly efficient solar cells on p-type EFG material at University of Konstanz (UKN) is very similar to industrial processing and is leading to a similar device structure. The lab-type process begins with a surface etch, followed by $POCl_3$ diffusion, PECVD SiN_x deposition, metallization and firing, and finally edge isolation. Main differences in lab-type processing are: smaller cell area (4 cm²); higher sheet resistance (80-100 Ω/sq) for better blue response; adapted optical parameters for SiN_x coating together with a second antireflection layer (MgF_2) giving a lower reflection and evaporated contacts using photolithography for lower shadowing and good contact resistances. In this contribution we show recent progress and studies in optimizing volume (hydrogenation and pregettering), front surface (plasma texturing and SiO_2/SiN_x front side passivation) and back side (first results for SiO_2/SiN_x back side passivation with laser fired contacts).

2 PHOTOLITHOGRAPHY PROCESS

2.1 Standard process

Figure 1 shows the conventional high efficiency process used at UKN for processing of multicrystalline material. The first step is a surface damage etch (chemical polishing etch based on HNO_3, HF and CH_3COOH; similar to CP6), followed by an optional pregettering step for potential bulk improvement ($POCl_3$ or BBr_3 at temperatures above 900°C with subsequent etch back of the diffused volume). For lowering the reflection a plasma texturing step can be implemented (either at IMEC or at UKN). Emitter diffusion is carried out in a conventional $POCl_3$ open tube diffusion followed by an optional oxidation (~ 10-15 nm SiO_2) for better front surface passivation before silicon nitride deposition by PECVD. An aluminum back surface field (Al-BSF) is formed by screen printing plus firing. After Al etching metallization is carried out using photolithography together with evaporation of contacts followed by silver plating. Finally the solar cells are cut out of the larger 5x5 cm² silicon substrate using a wafer dicing saw with subsequent contact sintering and hydrogenation by microwave induced remote hydrogen plasma (MIRHP). On selected samples a second antireflection layer (MgF_2) can be evaporated on top of the SiN_x.

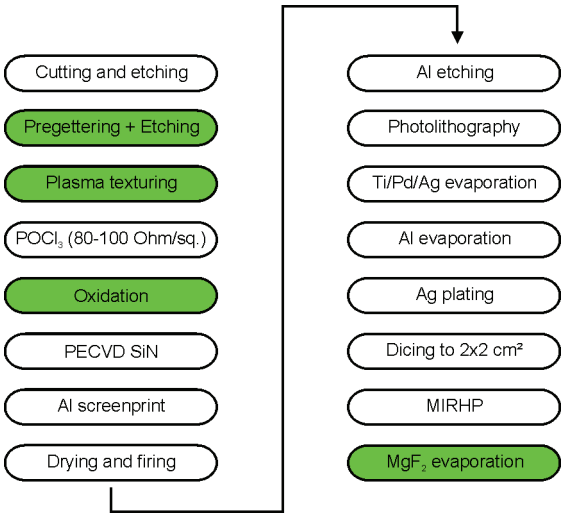

Figure 1: Standard high efficiency process for multicrystalline material used at UKN. Pregettering, plasma texturing, oxidation and MgF_2 evaporation are optional steps.

3 BULK IMPROVEMENT

3.1 Pregettering

In principle an additional pregettering step before the real emitter diffusion is able to improve bulk quality of multicrystalline material. However, high temperature steps (e.g. dry oxidation above 1000°C) can severely degrade the multicrystalline material. The effect of two different diffusions with similar thermal load differing mainly by the dopant source (BBr_3 and $POCl_3$) as a pregettering step was investigated. These two steps were compared to each other and to a reference without any pregettering step. The processing sequence is shown in figure 1 (oxidation and plasma texturing were not applied). Adjacent EFG wafer pairs as well as neighboring block cast multicrystalline wafers were investigated. The BBr_3 and $POCl_3$ diffusions were carried out at 935°C.

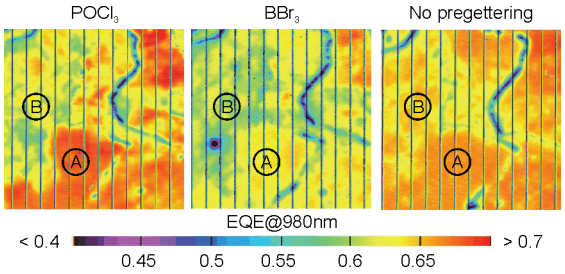

Figure 2: LBIC measurements for pregettering studies on neighboring block cast multicrystalline solar cells. Several regions (A, B) show different behaviour for the three chosen processes.

Differences between the pregettering conditions are most pronounced inside the different types of grains whereas only minor differences are visible at grain boundaries. This indicates a redistribution of impurities at high temperatures as expected. Although the thermal load during BBr_3 and $POCl_3$ diffusion is similar, the BBr_3 treated solar cells show lower EQE values in many areas most probably caused by a less efficient external gettering to the diffused surface. The comparison of the $POCl_3$ pregettered solar cell with the non-pregettered solar cell is interesting. Some areas (A) show a benefit from the pregettering, however, some other areas (B) show deterioration. Table I shows the IV data of the best solar cells featuring different pregettering steps.

The best solar cells on EFG material (2-3 Ωcm, ~300 µm) as well as block cast multicrystalline material (1 Ωcm, ~300 µm) reach the efficiency limit of the solar cell structure determined by floatzone references (~0.8 Ωcm, 210 µm) regardless if $POCl_3$ pregettering was used or not. As expected from the LBIC results presented in figure 2, the solar cells with a BBr_3 pregettering are less efficient. However, the solar cells "EFG (none)" and "EFG ($POCl_3$)" are adjacent but "EFG (BBr_3)" is not and thus these cells cannot be compared directly with each other.

All 3 EFG solar cells presented in table I received a second layer antireflection coating (MgF_2). IV data are presented in table II. Problems with contacting of uneven EFG solar cells can affect the correct measurement of fill factor, open circuit voltage and cell temperature during IV measurement.

Table I: IV values of the best solar cells (flat surface) featuring different pregettering steps. Measurements are carried out before evaporating a second layer of antireflection coating (MgF_2).

Material (pre-gettering)	FF [%]	j_{sc} [mA/cm²]	V_{oc} [mV]	η [%]
mc (none)	80.8	33.6	634	17.2
mc ($POCl_3$)	80.1	33.7	631	17.0
mc (BBr_3)	79.6	33.3	623	16.5
FZ (none)	80.9	33.6	629	17.1
EFG (none)	79.6	34.2	626	17.0
EFG ($POCl_3$)	79.9	34.4	625	17.2
EFG (BBr_3)	79.4	33.7	612	16.4

Table II: IV values of the best EFG solar cells after deposition of the second layer antireflection coating (SiN/MgF_2) together with the certified data of JRC Ispra.

Material (pre-gettering)	FF [%]	j_{sc} [mA/cm²]	V_{oc} [mV]	η [%]
EFG (none) UKN	79.2	36.4	628	18.1
EFG (none) JRC	80.0	36.0	623	17.9
EFG ($POCl_3$)	78.7	36.8	626	18.1
EFG (BBr_3)	79.4	36.0	615	17.6

3.2 Firing of PECVD SiN_x and screen printed Al

Experiments using EFG material [1] showed a considerable effect of the temperature profile during rapid thermal annealing of a hydrogen-rich PECVD SiN_x layer with screen printed Al on the back side. A fast firing with a peak temperature of about 750°C for only 1 second was suggested as optimized parameter. Recent investigations were carried out at UKN using a standard belt furnace instead of a RTP furnace with varying peak temperatures for comparison with the RTP results. Figure 3 shows the chosen process for the analysis.

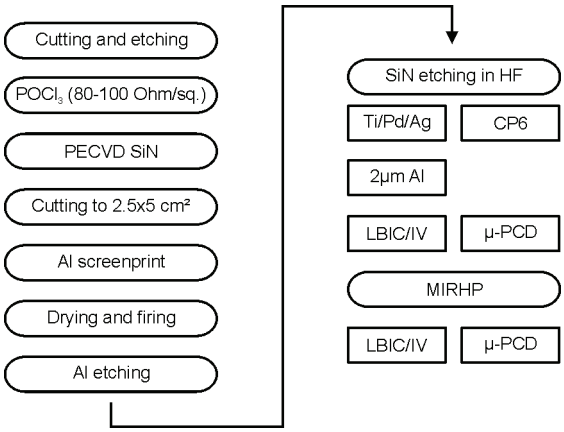

Figure 3: Modified process to investigate the influence of peak temperature during firing on adjacent wafers. Half of the wafers were etched back for bulk lifetime measurements using iodine/ethanol as surface passivation. The other half of the wafers was processed to solar cells for LBIC/IV analysis. Front contacts were evaporated using a shadow mask. The surface is not passivated and has no antireflection coating.

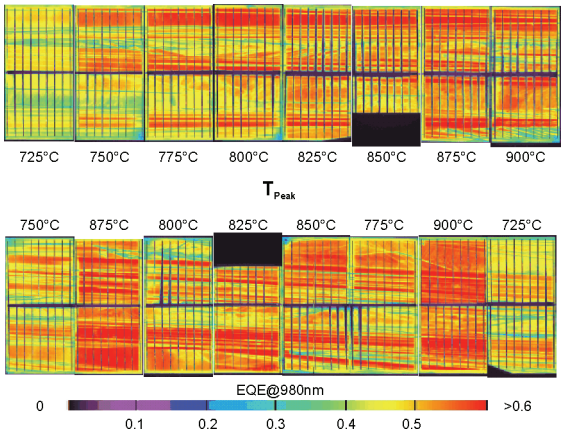

Figure 4: LBIC measurements of adjacent 2.5x5 cm² EFG solar cells fabricated with different peak temperatures (belt furnace set points) during SiN_x and Al firing. In the upper row firing temperature is increasing monotonously along crystallization direction. The lower row shows alternating firing temperatures.

Figure 4 shows a strong enhancement of bulk quality with increasing firing peak temperature (given are belt furnace set-points, not resulting wafer temperature). However, the lifetime analysis within the same experiment (figure 3, right column, results not shown here) revealed no visible effect of the firing temperatures on bulk lifetime. Up to now this result could not be explained. One reason could be an improvement of the diffusion constant of the minority carriers not affecting their lifetime. This could explain an improvement of the IV data without reflecting a bulk improvement by µPCD measurements. However, this is not very likely but can be checked in principle by Hall measurements.

Solar cells from neighboring block cast multicrystalline wafers simultaneously processed according to figure 1 (without pregettering, oxidation, texturing and MgF_2) showed a strange behavior, too (table III).

Table III: Mean V_{oc} values of neighboring block cast mc solar cells (4 2x2 cm² cells for each temperature). Additional values at 725°C (2 cells) and 900°C (4 cells) on floatzone references are presented to show the Al BSF effect.

T_{Peak} [°C]	**725**	**750**	**775**	**800**
V_{oc} [mV] (mc)	617	630	624	628
T_{Peak} [°C]	**825**	**850**	**875**	**900**
V_{oc} [mV] (mc)	628	628	624	625
T_{Peak} [°C]	**725**	**900**		
V_{oc} [mV] (FZ)	623	632		

The FZ references presented in table III are not expected to be influenced by hydrogenation. Thus the difference in V_{oc} is suspected to be caused by a different Al BSF. Neglecting the odd results at 750°C for the mc solar cells there seems to be an optimum in the range of 800-850°C.

These results show that even without the presence of a screen printed front side screen printed metallization the cell parameters are strongly related to the temperature profile of the firing step on all investigated materials (in industrial application the firing profile is essential to form a good emitter contact for the screen printed front metallization, restricting the allowed temperature range during firing). This is caused by a different effectiveness of hydrogenation as well as a different effectiveness of the Al BSF formation. Especially at elevated firing peak temperatures the Al BSF appears to be inhomogeneous as presented earlier [2]. It is likely that there exists an optimal firing condition for Al BSF formation and hydrogenation. The optimal temperature profiles for both purposes can vary for different materials and should be a topic for further investigations to address the inconsistency in the recently obtained measurement data.

With a different rear side passivation (as e.g. SiO_2/SiN_x) this optimization problem could be overcome (see chapter 5).

4 FRONT SIDE IMPROVEMENT

4.1 SiO_2/SiN_x stack for emitter passivation

Earlier results showed an improvement of the IV data using a thin thermal oxide underneath the front side PECVD SiN_x [3] on different materials for the process in figure 1. On EFG material this leads to a slight improvement compared to the cells presented in table II. In contrast to figure 4 the lower firing temperature leads to better results. The best EFG solar cell shows an efficiency of 18.2 %. Spectral response data of the adjacent EFG solar cell (18.1 % in efficiency) is presented in figure 9.

Table IV: IV data of 2 adjacent EFG solar cells with SiO_2/SiN_x front side passivation using different firing temperatures.

T_{Peak} [°C]	**FF [%]**	**j_{sc} [mA/cm²]**	**V_{oc} [mV]**	**η [%]**
875 (SiN_x)	78.1	33.5	623	16.3
825 (SiN_x)	78.5	34.2	628	16.9
825 (SiN_x/MgF_2)	79.3	36.4	632	18.2

4.2 Plasma texturing

Compared to other materials texturing on EFG material is a challenging task. Mechanical texturing is not feasible due to breakage. Common wet chemical texturing methods used for monocrystalline material are not applicable due to random grain orientations in multicrystalline materials. And for acidic wet chemical texturing methods for multicrystalline materials saw damage is needed for successful texturing [4]. EFG, however, is free of saw damage due to its unique crystallization method growing the wafers directly out of a silicon melt with the help of a shaping tool. Some texturing methods on String Ribbon material have been published reducing the reflectance but not improving cell efficiency due to increased recombination mechanisms at the textured surface [5].

Recent experiments showed progress using a SF_6 based plasma texturing (only on the front side of the wafer) applied at IMEC [6].

Table V: IV data of best adjacent EFG solar cells and floatzone references before and after MgF_2 deposition. PT: solar cells with plasma texturing applied at IMEC.

SiN_x	FF [%]	j_{sc} [mA/cm²]	V_{oc} [mV]	η [%]
FZ (flat)	81.0	32.9	635	16.9
FZ (PT)	81.0	34.8	635	17.9
EFG (flat)	79.0	32.5	608	15.6
EFG (PT)	80.0	34.3	610	16.7
SiN_x/MgF_2				
FZ (flat)	81.0	35.4	637	18.3
FZ (PT)	81.0	36.3	636	18.7
EFG (flat)	78.5	35.2	609	16.8
EFG (PT)	79.0	35.8	611	17.3

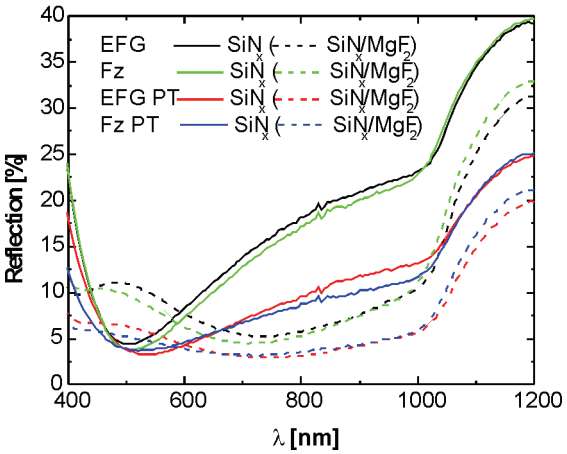

Figure 5: Reflection curves before and after MgF_2 deposition of the solar cells presented in table V. A significant reduction of the reflectance could be reached with the help of the plasma texturing applied at IMEC.

In some cases using a texturing within the UKN high efficiency process (figure 1) resulted in a decrease of fill factor and open circuit voltage (in industrial applications fill factor often increases using a texturing due to increased contact area reducing contact resistance). However, the plasma texturing at IMEC seems to affect neither fill factor nor open circuit voltage negatively. This results in an efficiency increase by plasma texturing of about 1 $\%_{abs}$ before and of about 0.5 $\%_{abs}$ after MgF_2 deposition on floatzone references as well as on EFG material. Encouraged by this results work is in progress to establish plasma texturing at UKN. First results are presented in table VI.

Table VI: IV data of best EFG solar cells and floatzone references before and after MgF_2 deposition. PT: solar cells with plasma texturing applied at UKN.

SiN_x	FF [%]	j_{sc} [mA/cm²]	V_{oc} [mV]	η [%]
FZ (flat)	80.9	33.3	635	17.1
FZ (PT)	80.6	34.8	631	17.7
EFG (PT)	80.0	34.2	603	16.5
SiN_x/MgF_2				
FZ (flat)	81.1	36.0	638	18.6
FZ (PT)	80.9	36.4	633	18.6
EFG (PT)	80.3	35.6	605	17.3

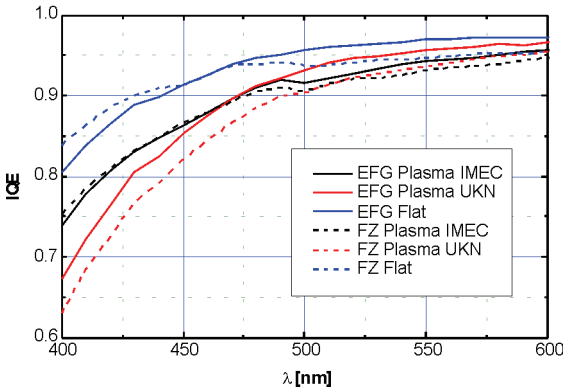

Figure 6: Spectral response data of EFG and FZ solar cells. Presented are flat cells (table V), plasma textured cells at IMEC (table V), and plasma textured cells at UKN (table VI). Concerning front surface recombination the plasma texturing applied at IMEC shows less recombination activity than the UKN texture but more than a flat surface.

The plasma texturing at UKN results in similar reflection behaviour compared to the plasma texturing applied by IMEC. Thus a significant improvement is realized if only a single layer of antireflection coating is used. However, for the floatzone references the solar cells with and without plasma texturing are of similar quality after evaporation of MgF_2. The reason is an increased surface recombination for the textured cells visible in the spectral response data.

Figure 6 indicates that the IMEC texture gives a slightly increased front surface recombination compared to the flat surface. The increased recombination is even more pronounced for the UKN texture explaining the differences in the IV data between both textures after MgF_2 evaporation (table V and VI).

Figure 7 shows the microscopic differences of both plasma textures.

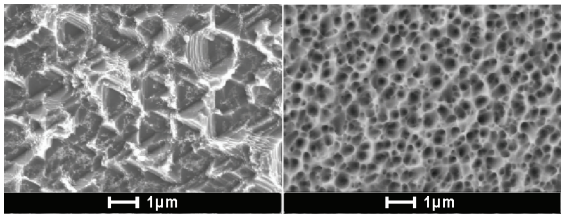

Figure 7: SEM images of plasma textures on EFG wafers (IMEC left, UKN right). Different topology is observed. Whereas the IMEC plasma texturing is more like a V-structure the UKN plasma texturing is spongy.

The sponginess of the UKN texture could be the reason for the lowered V_{oc} and j_{sc} compared to the excellent IMEC texture. An improved surface passivation (e.g. SiO_2/SiN_x stacks for emitter passivation) might help reducing this problem and is currently under investigation.

5 REAR SIDE IMPROVEMENT

5.1 SiO_2/SiN_x stack for rear side passivation

Recent studies [7] indicated that firing a both-sided hydrogen-rich PECVD SiN_x layer is able to significantly improve hydrogenation of multicrystalline material. But problems with a reliable dielectric rear surface passivation avoided improvements in cell efficiency using this cell design (figure 8) at UKN so far. Therefore fundamental studies on dielectric rear side passivation have been carried out on floatzone and multicrystalline wafers. These investigations will give input for implementation on EFG material in the future.

Table VII shows calculated surface recombination velocity (SRV) values after both-sided PECVD SiN_x deposition onto the thin thermal oxide, after a subsequent firing step in a conventional belt furnace and after an anneal at moderate temperatures (350°C) using MIRHP.

Table VII: SRV values of a SiO_2/SiN_x passivated floatzone reference (~ 0.8 Ωcm, 210 µm) after different steps without metallization.

Step	τ_{eff} [µs]	SRV [cm/s]
SiO_2/SiN_x	200	< 50
firing (> 750°C)	150	< 65
anneal (~ 350°C)	330	< 30

µ-PCD measurements reveal a homogeneous passivation of sample wafers. Thus the cell design (figure 8) can be realized with a suitable rear side passivation to increase cell efficiencies compared to the full area Al BSF process (figure 1).

The chosen process for the desired cell design (figure 8) is suitable for multicrystalline material including an effective hydrogenation step. First experiments with the improved cell process have been carried out on FZ references as well as on block cast mc material (Solsix). In contrast to commonly reported results the high temperature stability of such stacks was maintained.

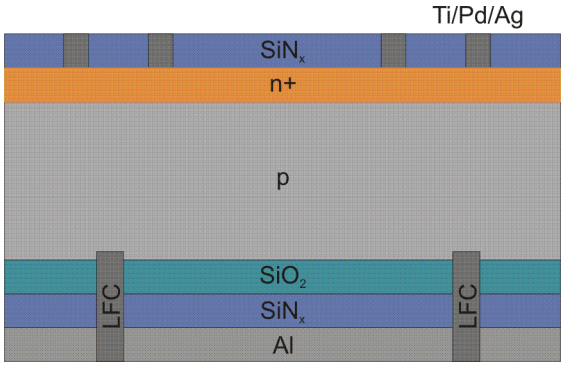

Figure 8: Solar cell design with improved rear side passivation using LFC technology (e.g. process reported in [7]).

Table VIII: IV data of best FZ and mc solar cells using the cell design illustrated in figure 8. The solar cells do not have any texturing and are cut out of the silicon substrate to 2x2 cm² using a dicing saw.

SiN_x	FF [%]	j_{sc} [mA/cm²]	V_{oc} [mV]	η [%]
FZ	78.9	34.7	653	17.9
mc	78.2	34.5	640	17.2
SiN_x/MgF_2				
FZ	79.2	37.4	655	19.4
mc	78.4	37.0	639	18.5

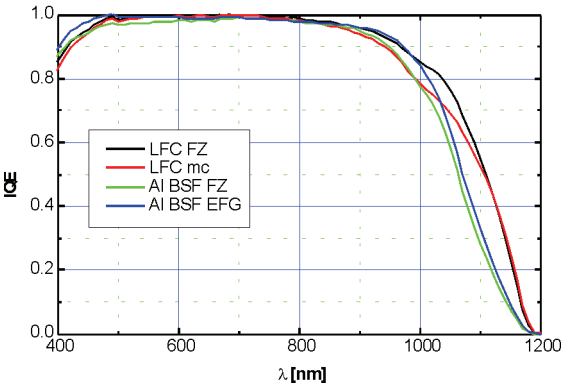

Figure 9: Spectral response data of solar cells with SiO_2/SiN_x passivated rear surface (LFC, table VIII) and of solar cells with full area Al BSF passivation (FZ reference, adjacent EFG solar cell to 18.2 % cell presented in table IV). Only the EFG solar cell has a SiO_2/SiN_x passivated emitter providing a better blue response as expected compared to the SiN_x front side.

Concerning the cells with full area Al BSF the EFG solar cell shows a better effective diffusion length (L_{eff}) compared to the FZ solar cell (figure 9). A possible explanation is the lower dopant concentration for the EFG material giving a more effective Al BSF passivation. However, a significant increase of L_{eff} is observed using the SiO_2/SiN_x passivated rear side of the FZ reference.

6 SUMMARY AND OUTLOOK

Bulk improvement experiments indicated that the investigated pregettering steps (at higher temperatures than standard emitter diffusion) are not beneficial for EFG as well as for the standard block cast multicrystalline material under investigation.

Firing temperatures during Al BSF formation seem to strongly affect the effectiveness of hydrogenation with the tendency of an improvement towards higher temperatures. In addition, the temperature profile may affect the Al BSF formation. It is not yet clear which is the optimum temperature profile for processing of multicrystalline material during Al BSF formation including hydrogenation (neglecting the narrow temperature range allowed for firing of the screen printed front metallization in industrial application). The optimal firing process is assumed to be different for various materials and has to be optimized individually.

Applying a cell process with full area rear side Al BSF passivation, EFG and block cast mc material are able to close up to the efficiency limit of such processes determined by floatzone reference material. 17.9 % efficiency was certified by JRC Ispra for the best EFG solar cell. With improved front surface passivation using a SiO_2/SiN_x stack the efficiency was further increased up to 18.2 %. This would be at the same level as the best reported solar cells on EFG material so far [8].

With the application of plasma texturing further increase of efficiencies on EFG material is possible, especially if only a single layer of antireflection coating is used.

Most benefit is expected using a SiO_2/SiN_x stack system for rear side passivation. The chosen process at UKN is suitable for multicrystalline material including an effective hydrogenation step with a high temperature stable rear side passivation. Combining the recent improvements, a further increase in cell efficiency for EFG material is expected in the future.

7 ACKNOWLEDGEMENTS

The underlying project of parts of this report was supported with funding by the EC (SES6-CT-2003-502583) and by the BMU (0327650H). The content of this publication is the responsibility of the authors.

8 REFERENCES

[1] A. Rohatgi, D.S. Kim, V. Yelundur, K. Nakayashiki, A. Upadhyaya, M. Hilali, V. Meemongkolkiat, Technical Digest of the 14th PVSEC, Bangkok 2004, p. 635

[2] F. Huster, G. Schubert, 20th EUPVSEC, Barcelona 2005, p. 1462

[3] M. Kaes, G. Hahn, Th. Pernau, A. Metz, 20th EUPVSEC, Barcelona 2005, p. 1063

[4] A. Hauser, I. Melnyk, E. Wefringhaus, F. Delahaye, G. Vilsmeier, P. Fath, 19th EUPVSEC, Paris 2004, p. 1094

[5] G. Hahn, I. Melnyk, C. Dubé, A.M. Gabor, 20th EUPVSEC, Barcelona 2005, p. 1438

[6] H.F.W. Dekkers, F. Duerinckx, L. Carnel, G. Agostinelli, G. Beaucarne, 21st EUPVSEC, Dresden 2006, p. 754

[7] M. Kaes, G. Hahn, A. Metz, 21st EUPVSEC, Dresden 2006, p. 679

[8] A. Rohatgi, D.S. Kim, K. Nakayashiki, V. Yelundur, B. Ronnsaville, APL (84)1, 2004, p. 145-147